

Origin of non-unique deprojection of the Galactic bar

HongSheng Zhao ^{*}

12 December 2017

ABSTRACT

Non-uniqueness of deprojecting the integrated light distribution of a nearby or faraway triaxial body is reviewed in the context of deriving the volume density of the Galactic bar from the COBE/DIRBE maps of the Galactic plane. The exact origin of this non-uniqueness is studied. One can write down a sequence of triaxial bar models which appear identical in integrated light from the Sun’s perspective, and the whole sequence is mapped out as a function of the Galactocentric distance of the observer from galactic to extragalactic distance scales. While mirror symmetries and perspective effects are compatible with any orientation of the bar in the sequence, weak upper and lower bounds can still be placed on the angles and axis ratios of the bar by positivity and other general requirements. Star count data of bulge giants are ideal for selecting a unique model from the sequence.

Key words: Galaxy: centre - Galaxy: structure - Gravitational lensing - galaxies: photometry - galaxies: kinematics and dynamics

1 INTRODUCTION

Deprojection of galaxies from the observed light distribution on the sky plane to the intrinsic 3D volume luminosity distribution is one of the basic problems of astronomy. It is common knowledge that the deprojected results are generally non-unique because of the freedom of distributing stars along any line of sight. General constraints such as symmetry, positivity and self-consistency are often too weak to completely break the degeneracy of models, in particular, the fundamental degeneracy of a triaxial ellipsoidal distribution vs an axisymmetric spheroidal one; both can project to the same elliptical isophotes in the line-of-sight integrated light distribution (Contopoulos 1956). Kinematic information such as rotation around the apparent minor/major axes of the isophotes and the 2D projected velocity field is necessary to solve this so-called “shape problem” of elliptical galaxies (Binney 1985, Franx, Illingworth & de Zeeuw 1991, Statler 1994 and references therein).

Nevertheless, as Blitz & Spergel (1991) pointed out in the case of the Galactic bar vs. an oblate bulge, the degeneracy is at least partially broken by photometric information from the perspective effect of nearby triaxial or bi-symmetric objects, namely with mirror symmetry with respect to three orthogonal planes. Perspective is the basis for the detection of the Galactic bar in the maps of the Galactic plane made by the DIRBE experiment aboard the COBE satellite. The dust-corrected infrared maps from COBE show significant systematic brightness variations between the right hand side

($l > 0^\circ$) and the left hand side ($l < 0^\circ$), and small systematic differences between the lower ($b < 0^\circ$) and the upper ($b > 0^\circ$) Galactic plane (Weiland et al. 1994): a strong signature of a nearly edge-on (mirror symmetry with the $b = 0^\circ$ plane) triaxial bar with the major axis of the bar rotated by an angle from our line of sight. A simple sketch of the geometry is shown in the top left diagram of Fig.1).

Dwek et al. (1995) made the first attempt to fit the COBE/DIRBE maps with a few simple analytical luminosity models. They found that the COBE maps are grossly consistent with several triaxial models: a very strong bar pointing almost along the Sun-Galactic center line of sight or a short bar pointing more sideways. Despite still significant residues of all their models, the existence of reasonable fits of the COBE map with a wide range of bar angles, axis ratios, radial profiles and degrees of boxyness suggest an intrinsic non-uniqueness among triaxial models which is not lifted by the perspective effect.

Binney & Gerhard (1996) separated the non-unique orientation of the bar from the likely unique 3D distribution once the three mirror planes of the bar are fixed. Their numerical experiments show that the final result of their non-parametric deprojection depends only on the assumed orientation of the bar, but not on the initial seed models for starting their Lucy-Richardson iterations. They explain the latter uniqueness as a compromise between the symmetry requirements of the density and a good fit to the perspective-induced asymmetries in the COBE map.

Binney, Gerhard & Spergel (1997) applied this non-parametric method to the COBE map after correcting for dust with an advanced extinction model from Spergel, Mal-

^{*} Sterrewacht Leiden (hsz@strw.LeidenUniv.nl)

hotra & Blitz (1997). They concluded that the major axis angle of the bar is likely very close to 20° with a good fit to the COBE map still possible for a positive smooth triaxial bar with major axis angle between 15° and 35° . They suspect that these limits on the bar angle mark the boundary of unphysical densities with negative regions and/or peculiar profiles.

Compared to external systems, perspective provides the unique signature for the Galactic bar as well as the subtleness to its non-uniqueness. The non-uniqueness in a nearby bar is entangled with perspective effects, making it a to-be-defined narrow sub-class of non-uniqueness for external systems. Simple transformations such as shearing/stretching an external ellipsoid in the line-of-sight direction can generate a sequence of ellipsoids with the same surface brightness map (Stark 1977, Franx 1988). But as Binney & Gerhard (1996) emphasize, moving material along the line of sight is forbidden by the mirror symmetries of a nearby bar. The well-known trick with axisymmetrical galaxies of adding a small amount of unphysical density with zero surface brightness (Rybicki 1986, Palmer 1994, Kochanek & Rybicki 1996, van den Bosch 1997, Romanowsky & Kochanek 1997), christened konuses by Gerhard & Binney (1996) for extragalactic axisymmetric bodies would not apply either. While preserving the orientation and the symmetry of the bar, adding konuses perturbs the left-to-right difference map.

Unfortunately none of the previous analyses with the COBE bar and external bars offer a satisfactory explanation for the non-uniqueness. In particular, the true source of non-uniqueness is never clearly singled out, and how this non-uniqueness varies as a function of the distance to the body is never clearly stated. It is also unclear how to transform one solution to another and map out the sequence of models admitted by the COBE maps, which is one of the main sources of information on the stellar distribution of the Galactic bar. Answers to such questions are important for integrating the constraints from the COBE map to other data of the bar from star counts, gas/stellar kinematics, and microlensing (see de Zeeuw 1993, Gerhard 1995). For example, the angle of the bar is a main source of uncertainty in comparing the COBE map with observed microlensing optical depth of the bar (Zhao & Mao 1996, Bissantz, Englmaier, Binney & Gerhard 1997); it is also a main source of uncertainty in determining the number density of brown dwarfs in the Galactic bar using microlensing (Zhao, Rich and Spiegel 1996).

This paper gives an analytical description of the nature of the non-uniqueness in the nearby COBE bar and points out its main differences with non-uniqueness in external systems. I also show how the positivity of the distribution puts a loose limit on the bar models, and discuss the best methods to lift the remaining degeneracy.

2 THE NATURE OF NON-UNIQUENESS

In this section I will describe the sources of non-uniqueness purely in words and illustrations without getting into the more mathematical aspect of the problem, which will be supplemented in §3 together with some applications to the COBE bar.

2.1 Mirror symmetries vs. invisible densities

Consider for the time being only bars which are symmetric with respect to the $b = 0^\circ$ plane. Divide the Galactic bar and the COBE map into a left and a right part with the $l = 0^\circ$ plane, which passes the Sun-center line and the rotation axis of the Galaxy. When folded along the $l = 0^\circ$ line, the COBE/DIRBE Galactic plane map $I(l, b)$ can be decomposed into two independent maps: a difference map $I(l, b) - I(-l, b)$ by subtracting the $l < 0^\circ$ side from the $l > 0^\circ$ side, and an addition map $I(l, b) + I(-l, b)$ by adding up the two sides. These two maps are line-of-sight integrations of the odd and the even parts of the volume density ν of the inner Galaxy, ν_{odd} and ν_{even} , decomposed in terms of the symmetry with respect to the $l = 0^\circ$ plane. The difference map and ν_{odd} are anti-symmetric with $l = 0^\circ$ plane, the addition map and ν_{even} are left-to-right symmetric.

Non-uniqueness originates from the large degrees of freedom in fitting the left-to-right symmetric addition map $I(l, b) + I(-l, b)$ [†]: any even component, such as an axisymmetric bulge or disc, a long end-on bar (the major axis coincides with the Sun-center line), a short side-on bar (the middle axis coincides with the Sun-center line) look very much alike in projection. In fact, in subtracting the axisymmetric component from the end-on bar model, one makes an unphysical distribution with some negative density regions, which is similar to extragalactic konuses in the sense that its projected light intensity is exactly zero after integration over any line of sight. I shall call such left-to-right symmetric unphysical components “invisible densities” since superimposing them on the bar is undetectable in projected light. They are the sources of non-uniqueness.

An example of an invisible density is illustrated in the upper right corner of Fig.1, where I tailor the radial profile of a stratified ball-shaped bulge in such a way so to have the same angular size and projected intensity as a uniform cigar-shaped bar placed end-on. Subtracting the ball-shaped bulge from the cigar-shaped bar yields an invisible density. The thin dark ring in the bulge is a density peak, corresponding to the line of sight to the far edge of the cigar-shaped bar, a direction where the depth and the projected intensity of the bar are at maximum. The fall-off of density towards the edge of the bulge corresponds to the ever-decreasing depth of the cigar-shaped bar with increasing impact parameter of the line of sight. Now superimpose a finite fraction, say f , of this unphysical component on the COBE bar, say, it is an ellipsoidal bar with a Gaussian radial profile. While such an “operation” is invisible in the projected light, its result is a new density with generally so irregular isophotes that there is no specific symmetry plane.

When the mirror symmetries with respect to three given orthogonal planes are imposed on the density distribution of the bar, the forementioned “invisible operation” is nearly forbidden because of the general twist of the major axis position, but not always. The exception is, as shown in the enlarged lower diagram of Fig.1, when the superimposed end-on bar is a clone of the original bar, in which case the

[†] Deprojection of the difference map $I(l, b) - I(-l, b)$, which distinguishes a bar from an axisymmetric bulge, is assumed to give a unique odd solution ν_{odd} in this paper.

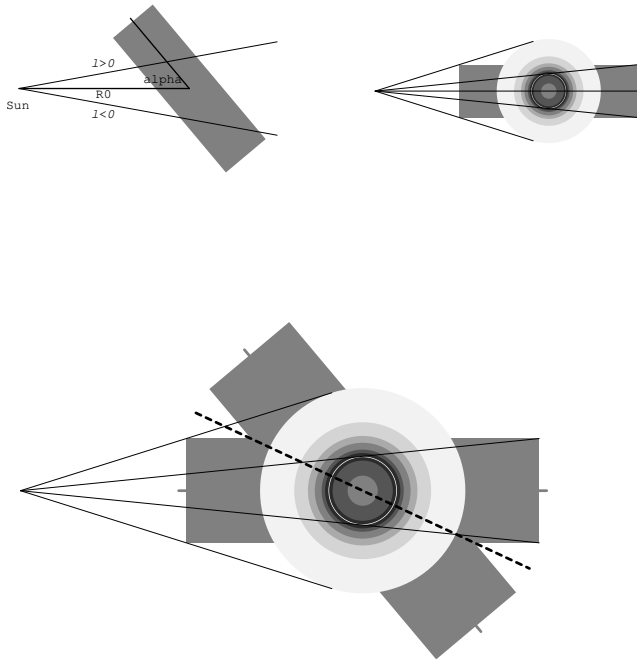


Figure 1. Crosssections of a uniform cigar-shaped bar tilted at an angle α from the Sun-center line (upper left), a two-component invisible density (upper right), and a superposition of the above two bodies (the enlarged lower diagram); several line-of-sight paths from the Sun are drawn in thin solid lines. The invisible density is made by subtracting from an end-on cigar-shaped bar a stratified ball-shaped bulge of the same angular size and projected intensity. Adding such an invisible density to the cigar-shaped bar on the upper left has no effect on the latter’s projected intensity, but rotates the mirror plane of the spatial distribution to the dotted line in the middle at an angle $\frac{\alpha}{2}$ from the Sun-center line.

final density should have mirror symmetry with respect to a new plane (the dotted line) which divides the angle of the Sun-center line and the major axis of the original bar in half. Namely the mirror symmetry is preserved, only the symmetry plane is different. Subtracting the round bulge has no further effect on the symmetry plane, but will take away any trace of transformation in the addition map of the integrated light. So *an invisible density which rotates and preserves mirror symmetry* is obtained by placing the original bar at end-on then subtracting off a round bulge. Generally the new major axis position depends on the fraction f of the added invisible density. When f is sufficiently small, the new density could also be positive everywhere. The general technique of designing invisible densities for a realistic triaxial bar is shown in §3.1 and §3.3, in particular, how to rotate the bar without twisting its major axis with radius.

2.2 Perspective effect, extinction and best-fit models

How is the perspective effect of the bar decoupled from the non-uniqueness problem? The perspective effect is only prominent in the difference map, and is by-passed by restricting all the transformations to the even part of the density: ν_{odd} is never affected by the invisible density. Still the invisible density is a function of the Galactocentric distance of the observer R_0 . For a hypothetical observer receding from the Galactic bar towards the anti-center, its Galactocentric distance R_0 increases, (the axisymmetric part of) the invisible density should be adjusted slightly to accommodate the changing perspective so to preserve this kind of non-uniqueness all the way to extragalactic distance. The common ambiguity of an extragalactic axisymmetric bulge with an end-on bar is a very special case of the kind of non-uniqueness with the COBE bar. As I will come back to in §3.2, *other distinctive features of the invisible density are that it has a net luminosity, it is not confined to any cone in the Fourier k -space and it is symmetric with respect to the $l = 0^\circ$ plane.*

Will invisible density remain invisible in the dusty Galaxy? Even at the near infrared the extinction of the COBE bar is a strong source of uncertainty for deprojection as shown by the strong color variation in the COBE/DIRBE maps (Arendt et al. 1994). In the first order approximation where dust is primarily situated in the foreground within the near 2 kpc of the line of sight to the center (Arp 1965), the projected intensity of the bar is simply multiplied by a reddening factor, thus the zero projected intensity of the invisible density is not affected. However at low latitude ($|b| \leq 3^\circ$) where dust and stars are mixed both in the disc and in the bar regions (Spergel, Maholtra & Blitz 1997), extinction will modulate the bar density with an ill-determined function for the dust distribution, which should be deprojected simultaneously with the stellar distribution. The invisible density, defined in the dust-free context, will cast faint (irregular) shadows on the COBE/DIRBE maps; one sees the near end of the end-on cigar-shaped bar (cf. upper right of Fig. 1) faintly in a heavy mist of interstellar dust. Although in principle one could still define a certain density which projects to zero after being modulated by dust, and infer the dust distribution from, say, star count data, independent of the to-be-deprojected maps, but finding such a density which preserves the triaxial symmetry of the bar becomes hopelessly difficult.

Do “best-fit” bar models mean anything? Since for any bar which fits the COBE/DIRBE maps, one can build a sequence of triaxial models with any bar angle to fit the data with exactly the same accuracy by adding different amount of the invisible density, *it is ill-defined to speak of the “best-fit” bar model or bar angle from the COBE/DIRBE maps.* The “best-fit” bar angles derived in the parametrized models of Dwek et al. are model dependent determinations. These, which could have fairly small error bars and/or residues (e.g. their G1, G2 and E3 models), are a mere reflection of the different ranges where their different *a priori* assumptions of the boxiness and radial profile of the density are “best” satisfied. The systematic residues in their models reflect only the unphysicalness of the *a priori* assumptions in detail (their diamond shaped bar is the best example). In fact it would

not even be surprising to have a perfect fit to the data for arbitrary bar angle (cf. eqs. 22- 23) provided the dereddened COBE maps are sufficiently smooth because there are in principle enough degrees of freedom in the mathematical functional forms of a triaxial density to make the problem underconstrained. It is straightforward to show that for observers nearby or at infinity this kind of ambiguity with the major axis angle occurs in every even m mode ($m = 2, 4, \dots$), odd m mode ($m = 1, 3, \dots$), and m -fold spiral arm mode where the major axis angle α also changes with R , and also in any band-limited superposition of finite number of modes. In all cases the major axis angle cannot be determined solely on the basis of the goodness of fit to the COBE map.

Then where do the limits for the bar angle come from? The only hope left to constrain the bar angle from the COBE maps is to impose some generally sensible unbiased requirements of the density, such as positivity, and to some extent smoothness, regular shape and radial profiles, as in Binney, Gerhard & Spergel (1997). An example is given in the following to illustrate the main points in this section.

3 APPLICATION TO THE COBE BAR

So far I have assumed that one can design invisible densities which project strictly to zero even for nearby bodies, and I have also restricted to the simple case that the observer is in the mid-plane of the bar. In this section some examples of the invisible density are written down as explicit functions of the observer's distance and viewing angles to the bar, allowing for a small vertical offset of the Sun from the mid-plane of the bar (Dwek et al. 1995, Binney, Gerhard & Spergel 1997). These toy models are used both to illustrate the non-uniqueness of the COBE bar and and to study possible methods to break the degeneracy.

3.1 An $m = 2$ bar viewed from a general distance and perspective

An $m = 2$ triaxial density distribution with any orientation of symmetry planes can be fairly generally written in a Galactocentric polar coordinate (r, θ, ϕ) as

$$\nu_{f=0}(r, \theta, \phi) = G(r) + P(r)H_{f=0}(\theta, \phi), \quad (1)$$

which is a superposition of a spherical component $G(r)$, and a triaxial perturbation with the radial profile $P(r)$ and the angular part $H_{f=0}(\theta, \phi)$; the latter equals to a function $H_f(\theta, \phi)$ evaluated at $f = 0$, where

$$\begin{aligned} H_f(\theta, \phi) \equiv & s_0 + (f + c_0) \cos^2 \theta \\ & + 2(c_1 \cos \phi + s_1 \sin \phi) \sin \theta \cos \theta \\ & + (c_2 \cos 2\phi + s_2 \sin 2\phi) \sin^2 \theta. \end{aligned} \quad (2)$$

One can show that the perturbation is triaxial since $r^2 H_{f=0}(\theta, \phi)$ reduces to a quadratic function in rectangular coordinates with ellipsoidal isosurfaces whose symmetry planes are determined by the constants c_0, c_1, c_2, s_0, s_1 , and s_2 .

Now a sequence of triaxial models with the same projected density as $\nu_{f=0}(r, \theta, \phi)$ can be made if one can write down its invisible density, which should be made by subtracting a spherical model from an end-on prolate bar with

amplitude $P(r)$. For convenience fix the pole of the Galactocentric polar coordinates (r, θ, ϕ) as the Sun-center line of sight, and the zero point of the roll angle ϕ as the $b = 0^\circ$ plane, so that in this coordinate system $P(r) \cos^2 \theta$ would describe an end-on prolate (i.e., ϕ -independent) distribution. Now suppose a spherical density $S(r)$ can be inverted[‡] from the integral equation,

$$\int_0^\infty S(r) dD = \int_0^\infty [P(r) \cos^2 \theta] dD \equiv T(l, b), \quad (3)$$

where $\int_0^\infty dD$ is an integration along any line-of-sight direction (l, b) , then

$$\nu_f(r, \theta, \phi) = \nu_{f=0}(r, \theta, \phi) + [P(r) \cos^2 \theta - S(r)] f, \quad (4)$$

describes a sequence (as function of the parameter f) of triaxial models with the same projected density. The sequence clearly preserves triaxial symmetry because like $\nu_{f=0}(r, \theta, \phi)$ of eq. 1

$$\nu_f(r, \theta, \phi) = [G(r) - fS(r)] + P(r)H_f(\theta, \phi), \quad (5)$$

also consists of a spherical component $G(r) - fS(r)$, and a triaxial perturbation with an angular dependence $H_f(\theta, \phi)$ similar to $H_{f=0}(\theta, \phi)$ (cf. eq. 2) except that the orientation of the symmetry planes will also depend on f .

By tuning solely f the model (cf. eq. 5) changes perspective with the Sun: the offset of the Sun from the mid-plane and the rotation of the major axis in the bar mid-plane are varied together along a 1D sequence. The less interesting third angle which describes a roll of the bar mid-plane around the Sun-center line, and is equivalent of the sky position angle in the case of extragalactic bodies, is not affected by adding an invisible density; the latter is invariant of a roll around the line-of-sight axis.

As a specific example to show how the model changes with the observer's distance and perspective, let

$$G(r) = \nu_0 \exp\left(-\frac{r^2}{2a^2}\right), \quad P(r) = \nu_0 \frac{r^2}{a^2} \exp\left(-\frac{r^2}{a^2}\right), \quad (6)$$

where a is the characteristic scale of the model. The spherical density $S(r)$, as specified in the integral eq. 3, can be solved analytically with a variation of the well-known Eddington formula for deprojecting spherical system.[‡] The dependence on the Galactocentric distance R_0 is generally such that if $S_\infty(r)$ is $S(r)$ in the limit of $R_0 \rightarrow \infty$ then $S(r) - S_\infty(r) \propto \left(\frac{a}{R_0}\right)^2$. For the models in eq. 6,

$$S(r) = S_\infty(r) \left[1 + \frac{a^2}{R_0^2} \left(\frac{2r^4}{a^4} - \frac{3r^2}{a^2} \right) \right], \quad S_\infty(r) = \frac{\nu_0}{2} \exp\left(-\frac{r^2}{a^2}\right), \quad (7)$$

[‡] Generally if $J(p)$ is the integrated intensity of the light distribution $S(r)$ or $P(r) \cos^2 \theta$ along a path with a Galactocentric impact parameter p , including the contributions from both the forward direction and the backward direction, $T(l, b)$ and $T(\pi + l, -b)$, then $J(p) \equiv T(l, b) + T(\pi + l, -b) \equiv \int_{-\infty}^\infty S(r) du = \int_{-\infty}^\infty P(r) \cos^2 \theta du$, where u is the offset along the line of sight from the tangent point, $r = \sqrt{p^2 + u^2}$, and $\frac{r \cos \theta}{p} = \left(\frac{u}{p} \sqrt{1 - \frac{p^2}{R_0^2}} - \frac{p}{R_0} \right)$. $S(r)$ is then inverted with an Abel transformation $S(r) = -\pi^{-1} \int_r^\infty \frac{dJ(p)}{dp} (p^2 - r^2)^{-1/2} dp$.

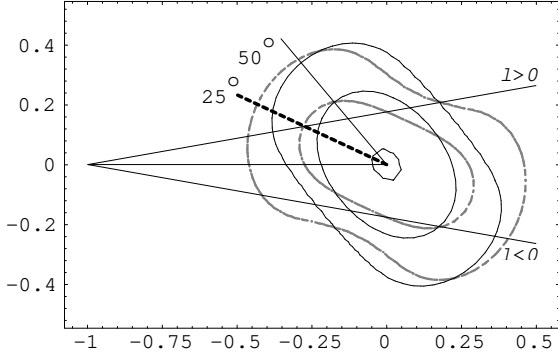


Figure 2. Equatorial slices of two triaxial models with identical surface brightness map, one at $\alpha = 25^\circ$ (thick dashed contours) and the other at $\alpha = 50^\circ$ (thin solid contours). The Sun is at $(-1, 0)$ to the central left. Two solid lines are drawn to show a line of sight at positive and negative longitude respectively.

and

$$\nu_f(r, \theta, \phi) = \nu_0 \exp\left(-\frac{r^2}{2a^2}\right) \left\{ 1 - \exp\left(-\frac{r^2}{2a^2}\right) \left[\frac{f}{2} + f \frac{r^2}{R_0^2} \left(\frac{r^2}{a^2} - \frac{3}{2} \right) - \frac{r^2}{a^2} H_f(\theta, \phi) \right] \right\}, \quad (8)$$

where the extra damping factor $\exp(-\frac{r^2}{2a^2})$ in front of the square bracket is to guarantee that the model is spherical and positive at large radius. The above equation yields triaxial models with monotonic and positive density and various degrees of flattening/triaxiality and boxyness for a wide range of scale length a and shape and perspective parameters $(c_0, c_1, c_2, s_0, s_1, s_2)$ and f . The models resemble the $G1$ and $G2$ models of Dwek et al. (1995) for the Galactic bar in terms of a Gaussian radial profile. Since the Sun is only about 10 pc from the midplane of the bar (Binney, Gerhard & Spergel 1997), the parameters s_1 and s_2 should be of the order $10\text{pc}/R_0 \sim 10/8000 \sim 0.01$, much smaller than unity. In particular, models with

$$s_1 = s_2 = 0, \quad f = c_2 - c_0 - 2c_1 \cot 2\alpha, \quad (9)$$

prescribe a sequence of edge-on (mirror symmetry with $b = 0^\circ$ plane) $m = 2$ perturbation, where α is the angle between the major axis of the perturbation and the $l = 0^\circ$ plane which passes the Sun and the rotation axis of the Galaxy. Fig.2 shows an equatorial slice of two such edge-on models from the sequence at $\alpha = 25^\circ$ and 50° respectively. The shape of bar is a function of the major axis angle such that models in a sequence yield the same projected light intensity from the Sun's perspective.

3.2 Non-uniqueness of the COBE bar vs. external systems

Now I digress from the COBE models to stress a few key differences between the non-uniqueness of the COBE models

and external systems. Unlike its external counterpart with $R_0 \rightarrow \infty$, the invisible density for a nearby triaxial body is not massless. For the bar models here, the invisible density has a mass proportional to $\frac{a^2}{R_0^2}$. The total luminosity of the bar models (cf. eqs. 8 and 2)

$$L \equiv \int d^3r \nu(r, \theta, \phi) = \pi^{\frac{3}{2}} \nu_0 a^3 \left[2^{\frac{3}{2}} + \frac{3s_0 + c_0}{2} - \frac{3}{2} \frac{a^2}{R_0^2} f \right], \quad (10)$$

changes with f .

To fit the same projected light intensity the models should have the same normalization ν_0 , but the total luminosity changes by a factor on the order of $\frac{a^2}{R_0^2} \sim$ a few percent for the COBE bars. This is because unlike external systems, the observed angular distribution of light in the COBE bar does not simply sum up to a unique measurement of its total luminosity. The result depends on knowing the distance to the bar and the orientation of the bar. The upper panel of Fig.3 shows that an observer at the Sun's position $R_0 = 8\text{kpc}$ may slightly underestimate/overestimate the intrinsic luminosity by about 10% depending on assumptions of the bar angle. Moving out to the anti-center the observer has a full outside view of the bar and hence a better determination of its luminosity but sacrifices somewhat tighter constraint on the bar angle from the perspective effect and positivity. Going to the center of the bar, the observer has full information of the orientation of the bar (the brightest direction is the major axis direction), but very poor information of the intrinsic luminosity profile and total luminosity.

Another feature of the invisible density here is that unlike konus-like structures, it is not confined to any cone in the Fourier \mathbf{k} -space even in the limit $R_0 \rightarrow \infty$. This is shown explicitly by computing the Fourier transform of the (prolate band-limited) invisible density (cf. eqs. 6 and 7) using eqs. 4, 24 and 25 of Palmer (1994).

$$F(\mathbf{k}) \equiv \int d^3r \exp(-i\mathbf{k} \cdot \mathbf{r}) [P(r) \cos^2 \theta - S(r)] \quad (11)$$

$$= F_{R_0 \rightarrow \infty}(\mathbf{k}) + \frac{a^2}{R_0^2} T(k), \quad (12)$$

which is a \mathbf{k} -space prolate distribution around the Sun-center line, where

$$F_{R_0 \rightarrow \infty}(\mathbf{k}) \equiv \pi^{\frac{3}{2}} \nu_0 a^3 \left(\cos^2 \theta_{\mathbf{k}} - \frac{2}{3} \right) \frac{k^2 a^2}{4} \exp\left(-\frac{k^2 a^2}{4}\right), \quad (13)$$

$\theta_{\mathbf{k}}$ is the angle of the \mathbf{k} -vector with the Sun-center line, and

$$T(\mathbf{k}) \equiv \pi^{\frac{3}{2}} \nu_0 a^3 \left(-\frac{3}{2} + \frac{21k^2 a^2}{24} - \frac{k^4 a^4}{16} \right) \exp\left(-\frac{k^2 a^2}{4}\right). \quad (14)$$

One recovers the mass of the invisible density in the limit $\mathbf{k} \rightarrow 0$, $F(0) = \frac{a^2}{R_0^2} T(0) = -\frac{3a^2}{2R_0^2} (\pi^{\frac{3}{2}} \nu_0 a^3)$ (cf. eq 10). Eq. 13 shows that even when the bar is placed at infinity, $F(\mathbf{k}) = F_{R_0 \rightarrow \infty}(\mathbf{k}) \neq 0$ everywhere (except at $\mathbf{k} = 0$ and/or $\theta_{\mathbf{k}} = \cos^{-1} \sqrt{\frac{2}{3}}$). Since $F(\mathbf{k}) = 0$ for konus-like structures (or its triaxial version) outside a certain ‘‘cone of ignorance’’ around a principal axis of the model (Rybicki 1986, Gerhard & Binney 1996, Kochanek & Rybicki 1996), the kind of non-uniqueness shown in this paper has little to do with konuses. The two sequences of models meet only for an end-on prolate bar seen at infinity, which can alternatively be interpreted as an axisymmetric system with inclination $i = 0$ (face-on). In

this special case the invisible density here becomes a konus but the half opening angle of the “cone of ignorance” is as large as $\frac{\pi}{2}$.

The invisible density is also of different nature from the kind of non-uniqueness associated with a simple shear and/or stretch transformation of an ellipsoid. This applies even in the limit that the object is at infinity because these transformations normally change the odd part of the density, while the invisible density here is strictly an even function.

3.3 Limits on the bar angle vs. positivity

The limits for the bar angles are given by the positivity requirement. They can be derived analytically in the context of models more general than eq. 8 without additional effort. As it turns out, the results are simplest for the broad class of interesting edge-on models with an axisymmetric component and an m -mode perturbation; $m = 2, 4, \dots$ if mirror symmetry is imposed. These models have a density distribution which can be written with no loss of generality as

$$\nu_\alpha(R, z, \psi) = \left[A_\alpha(R, z) + \frac{B_m(R, z)}{\sin m\alpha} \cos m(\psi - \alpha) \right], \quad (15)$$

$$A_\alpha(R, z) \equiv C(R, z) - \cot m\alpha V_m(R, z), \quad (16)$$

$$K_m(R, z, \psi) \equiv [B_m(R, z) \cos m\psi - V_m(R, z)], \quad (17)$$

and

$$\int_0^\infty dDK_m(R, z, \psi) = 0, \quad (18)$$

where a Galactocentric cylindrical coordinate system (R, z, ψ) is used with the azimuthal angular coordinate ψ counted from the $l = 0^\circ$ plane; the major axis of the perturbation is along $\psi = \alpha$ with amplitudes $\frac{B_m(R, z)}{\sin m\alpha}$, where $B_m(R, z)$ specifies the odd part of the density (cf. eq. 23), and $C(R, z)$ is an axisymmetric fit to the addition map (cf. eq. 22), and $K_m(R, z, \psi)$ is an invisible density, made by subtracting an axisymmetric component $V_m(R, z)$ from an end-on bar $B_m(R, z) \cos m\psi$.

A few brief comments before proceeding to derive the limits on the bar angle. Eqs. 15- 18 imply that any triaxial bar with the same amplitudes $C(R, z)$ and $B_m(R, z)$ will follow a sequence with identical line-of-sight integrated light distributions on both positive and negative l sides $I(\pm l, b)$, the same odd parts ν_{odd} (with respect to the $\psi = l = 0^\circ$ plane) in density, and different even parts ν_{even} , but with the difference being a linear superposition of invisible densities $K_m(R, z, \psi)$. For triaxial densities with generally multiple modes ($m = 2, 4, \dots$), they are related to each other by an invisible density

$$\sum_{m=2,4,\dots} (\cot m\alpha' - \cot m\alpha) K_m(R, z, \psi), \quad (19)$$

where the sum of different modes in the given proportion is necessary to prevent spiral-arm-like twist of the major axis. Adding this invisible density to a model with symmetry plane at $\psi = \alpha$ rotates the plane to $\psi = \alpha'$. The sequence of edge-on models given by eq. 5 and 9 is a subclass of the models here with $m = 2$, and

$$B_2(R, z) = -c_1 P(r) \frac{R^2}{r^2}, \quad V_2(R, z) = -2c_1 S(r) - B_2(R, z), \quad (20)$$

$$C(R, z) = G(r) + (c_0 - c_2) S(r) + P(r) \left(s_0 - c_2 + 2c_2 \frac{R^2}{r^2} \right). \quad (21)$$

Generally $C(R, z)$ and $B_m(R, z)$ should be derived from fitting the addition and the difference maps of the projected light,

$$\frac{1}{2} [I(l, b) + I(-l, b)] = \int_0^\infty C(R, z) dD, \quad (22)$$

$$\frac{1}{2} [I(l, b) - I(-l, b)] = \int_0^\infty B_m(R, z) \sin m\psi dD, \quad (23)$$

and $V_m(R, z)$ from eq. 17.

Impose positivity requirements to $\nu_\alpha(R, z, \psi)$,

$$A_\alpha(R, z) \equiv [C(R, z) - \cot m\alpha V_m(R, z)] \geq \frac{B_m(R, z)}{\sin m\alpha} \quad (24)$$

for all (R, z) . This reduces to an upper and a lower bound for the angle α ,

$$\text{Max}[t_-] \leq \tan \frac{m\alpha}{2} \leq \text{Min}[t_+], \quad (25)$$

where $t_- \leq t \leq t_+$ is the range bounded by the effectively quadratic inequality for a variable t

$$\frac{B_m - V_m}{2C} t + \frac{B_m + V_m}{2C} t^{-1} \leq 1 \quad (26)$$

at a given position (R, z) on the meridional plane, and the overlapped interval of these ranges is used in eq. 25. The exact upper and lower bounds of the angle α for the COBE bar will be discussed elsewhere as it involves solving three integral equations numerically (eqs. 22 and 23 for $B_m(R, z)$ and $C_m(R, z)$ and eq. 17 for $V_m(R, z)$), and several practical issues not considered so far (including a detailed dust model for the COBE/DIRBE maps, the choice of fitting regions with reliable photometry, the degree of smoothness of the solution in a non-parametric fit, and search of solutions in the 1D parameter space spanned by α). Here it is only worth commenting on two points. First Binney, Gerhard & Spergel (1997) showed that it is possible to obtain good fits to the COBE maps with a triaxial bar if the bar angle is in the range $15^\circ \leq \alpha \leq 35^\circ$ and the Sun is very close the midplane of the bar. A sequence of models which is roughly consistent with these limits is discussed in the next section. Second the range for α is set by C_m and B_m , which are in turn set by the addition map and the difference map respectively with an integration over the line of sight (cf. eq. 22 and 23). Hence the range for α is also a function of the distance to the bar. However, the upper and lower limits are only weakly dependent on the distance as long as the observer is outside the bar, as shown in Fig.3 by the nearly horizontal boundaries of the shaded region for $R_0 \gg 2$ kpc.

3.4 A toy model and implications to the COBE bar

To illustrate the non-uniqueness in the Galactic bar, and how to lift the degeneracy, consider edge-on models in eq. 8 and 2 with

$$a = 2 \text{ kpc}, \quad c_0 = c_2 = -\frac{c_1}{2} = \frac{1}{6}, \quad s_0 = -1, \quad (27)$$

and (cf. eq. 9)

$$s_1 = s_2 = 0, \quad f = c_2 - c_0 - 2c_1 \cot 2\alpha = \frac{2}{3} \cot 2\alpha, \quad (28)$$

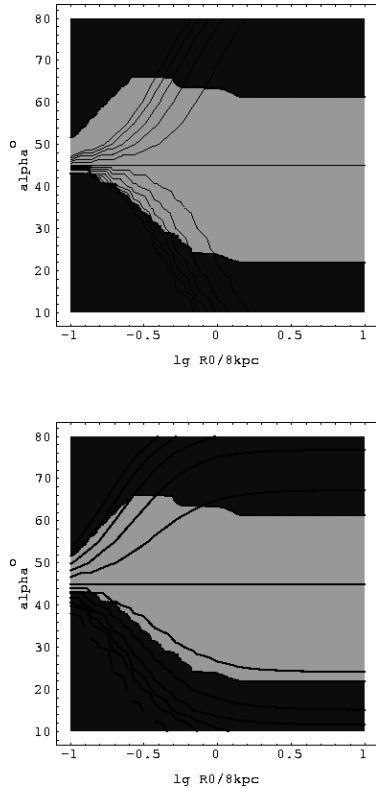


Figure 3. For an edge-on bar with a fixed M/L and parameters given in eq. 27, positivity of the density puts loose upper and lower limits on the bar angle (cf. eqs. 25, 26, 20 and 21). These limits are functions of the distance to the bar, which mark the upper and lower boundaries of the shaded region in the $\log(R_0/8\text{kpc})$ vs. α plane. The contours show the bar's absolute magnitude (upper panel) in the $\log(R_0/8\text{kpc})$ vs. α parameter plane with an interval of 0.05 magnitude, and the equal contours of the central escape velocity $\sqrt{2|\Phi(0)|}$ (lower panel) in intervals of 5%. Both the escape velocity and the luminosity increase with increasing α , but the increment is small as long as one is observing from well outside the bar, despite the strong ambiguity with the angle of the bar.

which prescribes a sequence of edge-on $m = 2$ bars with a Gaussian radial profile inside about 4 kpc of the center with major axis at an angle α from the Sun-center line. The density is strictly positive everywhere for models with a broad range of major axis angles, $22.5^\circ \leq \alpha \leq 63.5^\circ$ for $R_0 = 8$ kpc (cf. the shaded region in Fig. 3). Models are also monotonic everywhere except for a small bump near $\frac{R_0}{2} \sim 4$ kpc on the short and middle axes. These limits will be significantly relaxed when an axisymmetric exponential disc is included because it adds a positive background distribution; a disc with peak intensity about 1/10 of the bar can also make $\alpha \sim 15^\circ$ and $\alpha \sim 75^\circ$ models positive everywhere.

While the specific models here are clearly toy models, too simplistic to fit the COBE map in any detail, as shown in Fig.2, they grossly resemble the Galactic bar in terms of its Gaussian radial profile (Dwek et al. 1995), its shape and axis ratios. In particular, the range of the bar angle here is largely in agreement with those in the literature (see a table compiled in Gerhard 1995), including the results of

Binney, Gerhard & Spergel (1997) and Dwek et al. (1995) derived from fitting the COBE map, and Stanek et al. (1994, 1997) derived from fitting the star count data of bulge red clump giants. Hence the models are useful to demonstrate the non-uniqueness and test various techniques for lifting the non-uniqueness.

Fig.2 shows an equatorial slice of the model at $\alpha = 25^\circ$ (the thin peanut-shaped bar) in heavy dashed contours and a model at $\alpha = 50^\circ$ (the more concentrated bar) in solid contours. These two grossly different models look exactly the same in line-of-sight integrated intensity for an observer at $(-1, 0)$ at the central left (the assumed position of the Sun). Neither of these two models can be easily ruled out on the basis of stability and self-consistency.

Nevertheless it is possible to break the degeneracy with kinematic data since *the invisible density changes the orientation of the bar potential model as well as its shape and depth*. For the models in eq. 8, the depth of the potential well at the center is

$$|\Phi(0)| = \pi\nu_0 a^2 G(M/L) \left[\left(4 + 2s_0 + \frac{2}{3}c_0 \right) - \left(\frac{1}{3} + \frac{a^2}{R_0^2} \right) f \right], \quad (29)$$

which decreases linearly with increasing fraction (f) of the superimposed invisible density, where M/L is the mass-to-light ratio, assumed to be the same for all models. As a result, the potential well of the $\alpha = 25^\circ$ model is slightly shallower than that of the more centrally concentrated $\alpha = 50^\circ$ model (cf Fig.2). However, the difference is only 7% in term of the maximum escape velocity $\sqrt{2|\Phi(0)|}$ of the models (cf. lower panel of Fig.3). The differences in terms of the mass weighted average velocity dispersion (estimated from the virial theorem) and the circular velocity (estimated directly from the potential) are also at only a few percent level, too small to be measured with certainty. To distinguish the models with kinematic data, one needs to model the anisotropy and perspective effects of the bar orbits in detail, e.g., the longitude-velocity diagram for orbits of gas clouds (Binney et al. 1991, Zhao, Rich & Spergel 1996), and the vertex deviation in the stellar velocity ellipsoid (Zhao, Spergel & Rich 1994); these models introduce additional complexity such as the pattern speed of the bar, and the stellar distribution function.

The most straightforward approach to break the degeneracy of the COBE bars is perhaps to compare the models with measurements of the line of sight distance distribution of the bar from color-magnitude diagrams. The depth of the models, defined here as the rms dispersion of distance in the Sun-center line of sight, decreases from $0.26R_0$ for $\alpha = 22.5^\circ$ to $0.19R_0$ for $\alpha = 63.5^\circ$. The 30% difference is detectable with good distance indicators and large data sets, such as the bulge red clump giants in the microlensing and variable star surveys towards the Galactic bulge (Paczynski 1996). It is also interesting that *the invisible density also leaves observable traces on the microlensing maps*, i.e., the distribution of the optical depth on the sky plane (Evans 1995, Bissantz, Englmaier, Binney & Gerhard 1997). This is because the optical depth is proportional to both the projected intensity and the line-of-sight depth, and while an invisible density does not change the former, it changes the latter. The microlensing optical depth increases by about 50% by going from the $\alpha = 63.5^\circ$ model to the $\alpha = 22.5^\circ$ model. Nevertheless, since the data set on bulge red clump giants

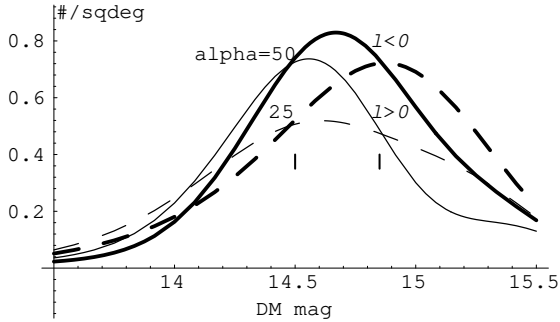


Figure 4. Simulated distance modulus distributions for red clump giants in the two bar models $\alpha = 25^\circ$ (dashed curves) and 50° (solid curves) in Fig. 2 at line of sight directions ($\pm 5^\circ, -4^\circ$).

is on the order of a million times larger than that of microlensed sources, it argues for the former plus the COBE map being the speediest approach. However, fitting the microlensing optical depth, gas/stellar velocities can set the normalization of the density, namely the mass-to-light ratio. To fit the same projected light intensity the models should have the same normalization ν_0 [§], but the total luminosity increases by about 8% (cf. eq. 10) by going from a $\alpha = 22.5^\circ$ model to a $\alpha = 63.5^\circ$ model.

Fig. 4 shows the simulated star count data for the two models at line of sight directions $(l, b) = (\pm 5^\circ, -4^\circ)$, with an assumed Galactocentric distance modulus (DM) 14.5 magnitude. The predictions have taken into account the growing volume with radius for a given solid angle, and have been convolved with the dispersion of the absolute magnitude of the clump giants (about 0.2 magnitude). The predicted distance modulus distributions are quite different for the two models in terms of the peak position, the width and shape of profiles. The fact that for both models the $l > 0^\circ$ side is closer than the $l < 0^\circ$ side is because the major axes of both bars are placed at positive α . Interestingly the amount of $l > 0^\circ$ vs. $l < 0^\circ$ asymmetry is the same for both models, as indicated by the two short vertical lines in Fig. 4, because the left-to-right symmetric invisible density has no effect on the asymmetry. The distributions resemble Fig. 2 of Stanek et al. (1994), which show the apparent magnitude distribution of Galactic bulge red clump giants at the same low-extinction line of sight directions ($\pm 5^\circ, -4^\circ$) in the OGLE microlensing surveys. While it is premature to use the simple analytical models here to draw any conclusion on the bar angle, they suggest that an integration of the COBE map with the star count data of bulge red clump giants (Stanek et al. 1997) can lift the degeneracy of the bar models.

[§] ν_0 is not the peak density $\nu(0) = \left(1 - \frac{f}{2}\right)\nu_0$ (cf. eq. 8), which roughly doubles by going from a $\alpha = 22.5^\circ$ model to a $\alpha = 63.5^\circ$ model.

4 CONCLUSION

The non-uniqueness in deprojecting the COBE/DIRBE maps originates from the simple fact that a round bulge can mimic an end-on bar in the line-of-sight integrated light distribution. This kind of non-uniqueness is almost lifted when bar-like reflection symmetries are imposed, except that the angle of these symmetry planes with our line of sight is still a free parameter, which can only be loosely constrained by the positivity of the deprojected density. The main results are summarized as follows. (1) Triaxial Galactic bar models, which project to identical intensity map in the absence of extinction, form a 1D sequence as function of the bar's orientation, in agreement with numerical results of Binney & Gerhard (1996). (2) It is ill-conditioned to speak of any best-fitting bar model because the limit on the bar parameters comes from plausibility of the density (positivity, smoothness, and regular-looking shape and radial profile, etc.), not from the goodness of fit. (3) The theory predicts that COBE models likely follow a sequence with identical ν_{odd} , which is uniquely constrained by the perspective effects of a triaxial bar. (4) The non-uniqueness in the even part of the density ν_{even} is of nature entirely different from those induced by shearing/stretching of an external ellipsoid (Stark et al. 1977) or adding a konus-like structure (Gerhard & Binney 1996). (5) Various methods to fully break the degeneracy of COBE bars are compared. In agreement with findings for extragalactic axisymmetrical systems (van den Bosch 1997, Romanowsky & Kochanek 1997), it is unlikely to put a very tight limit on the bar's parameter space with general dynamical constraints such as self-consistency and stability, but it is still hopeful to lift some degeneracy by fitting kinematic data of gas and stars with sophisticated dynamical models. With the increasing number of microlensing events towards the bulge, microlensing optical depth maps also have the potential of lifting the degeneracy of the models. But the cleanest approach to remove the ambiguity of the bar angle is to compare with star count data from the current bulge microlensing and variable star surveys, in particular the large data set on the bulge red clump giants, which provide the extra constraints on the "depth" of the bar (Stanek et al. 1997). Extinction is the main limiting factor in analysis of both star counts and COBE maps. Finally the mass-to-light ratio, the last parameter of a complete mass model of the bar, can be determined from fitting gas/stellar kinematics or the microlensing optical depth (Bissantz, Englmaier, Binney, & Gerhard 1997).

I thank Frank van den Bosch for a helpful discussion in the early stage of this work, Tim de Zeeuw and Ortwin Gerhard for a careful reading of an early draft.

REFERENCES

- Arp H. 1965, ApJ, 141, 43
- Arendt R.G. et al., 1994, ApJ, 425, L85
- Binney J.J. 1985, MNRAS, 212, 769
- Binney J.J., & Gerhard O.E., 1996, MNRAS, 279, 1005
- Binney J.J., & Gerhard O.E., & Spergel D.N. 1997, MNRAS, in press
- Binney J. et al. 1991, MNRAS, 252, 210
- Bissantz N., Englmaier P., Binney J.J., Gerhard O. 1997, MN, in press, (astro-ph/9612026).

- Blitz L. & Spergel D.N. 1991, ApJ, 379, 631.
 Contopoulos G. 1956, Z. Astrophys., 39, 126
 de Zeeuw P.T. 1993, in *Galactic Bulges*, Eds. H. Dejonghe and H.J. Habing (Kluwer Academic Publ.: Netherlands), p 191.
 Dwek E. et al. 1995, ApJ 445, 716
 Evans W. 1995, ApJ, 437, L31
 Franx M. 1988, ApJ, 231, 285
 Franx M., Illingworth G., de Zeeuw T.P. 1991, ApJ, 383, 112
 Gerhard O.E., 1995, in IAU symposium 165, "Unsolved Problems in the Milky Way", ed. L. Blitz (Dordrecht:Kluwer), p79
 Gerhard O.E. & Binney J.J., 1996, MNRAS 279, 993
 Kochanek C.S. & Rybicki G.B. 1996, MNRAS, 280, 1257
 Paczyński B. 1996, ARAA, 34, in press
 Palmer P.L. 1994, MNRAS, 266, 697
 Romanowsky A.J., Kochanek C.S. 1997, submitted to MNRAS (astro-ph/9609202)
 Rybicki G.B. 1986, in Structures and dynamics of elliptical galaxies, IAU Symp. 127, ed. de Zeeuw P.T., Kluwer, Dordrecht, 397
 Spergel D.N., Malhotra S., Blitz L. 1997, in preparation
 Stanek K.Z., Mateo M., Udalski, A., Szymański, M., Kaluźny, J., Kubiak, M. 1994, Ap.J., 429, L73
 Stanek K.Z., et al. 1997, ApJ, 477, 163
 Stark A.A. 1977, ApJ, 213, 236.
 Statler T.S., 1994, ApJ, 425, 458
 van den Bosch F.C. 1997, MNRAS, in press
 Weiland J. et al. 1994, ApJ, 425, L81.
 Zhao H.S. & Mao S. 1996, MNRAS, 283, 1197
 Zhao H.S., Rich R.M. & Spergel D.N. 1996, MNRAS, 282, 175
 Zhao H.S., Spergel D.N., & Rich R.M. 1994, AJ, 108, 6

This paper has been produced using the Royal Astronomical Society/Blackwell Science L^AT_EX style file.